Front. Environ. Sci. Eng. 2022, 16(4): 46
https://doi.org/10.1007/s11783-021-1480-9

RESEARCH ARTICLE

Tracing the impact of stack configuration on interface resistances in reverse electrodialysis by in situ electrochemical impedance spectroscopy

Wenjuan Zhang (✉)[1], Bo Han[2], Ramato Ashu Tufa[3], Chuyang Tang[4], Xunuo Liu[1], Ge Zhang[1], Jing Chang (✉)[1], Rui Zhang[1], Rong Mu[1], Caihong Liu[5], Dan Song[2], Junjing Li[6], Jun Ma[2], Yufeng Zhang[1]

1 Tianjin Key Laboratory of Aquatic Science and Technology, School of Environmental and Municipal Engineering, Tianjin Chengjian University, Tianjin 300384, China
2 State Key Laboratory of Urban Water Resource and Environment, Harbin Institute of Technology, Harbin 150090, China
3 Department of Inorganic Technology, University of Chemistry and Technology Prague, Technicka 5, 166 28, Prague 6, Czech Republic
4 Department of Civil Engineering, the University of Hong Kong, Hong Kong, China
5 Key Laboratory of Eco-environments in Three Gorges Reservoir Region (Ministry of Education), School of Urban Construction and Environmental Engineering, Chongqing University, Chongqing 400044, China
6 School of Environmental Science and Engineering, Tianjin Polytechnic University, Tianjin 300387, China

HIGHLIGHTS

- RED performance and stack resistance were studied by EIS and LSV.
- Interface resistance were discriminated from Ohmic resistance by EIS.
- Impacts of spacer shadow effect and concentration polarization were analyzed.
- Ionic short current reduced the power density for more cell pairs.
- The results enabled to predict RED performance with different configurations.

GRAPHIC ABSTRACT

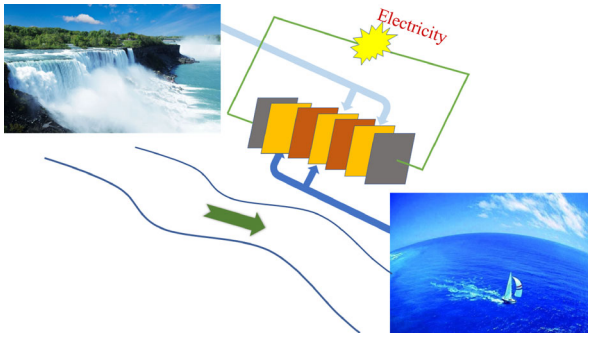

ARTICLE INFO

Article history:
Received 31 March 2021
Revised 31 May 2021
Accepted 27 June 2021
Available online 13 August 2021

Keywords:
Reverse electrodialysis
Electrochemical impedance spectroscopy
Concentration polarization
Spacer shadow effect

ABSTRACT

Reverse electrodialysis (RED) is an emerging membrane-based technology for the production of renewable energy from mixing waters with different salinities. Herein, the impact of the stack configuration on the Ohmic and non-Ohmic resistances as well as the performance of RED were systematically studied by using in situ electrochemical impedance spectroscopy (EIS). Three different parameters (membrane type, number of cell pairs and spacer design) were controlled. The Ohmic and non-Ohmic resistances were evaluated for RED stacks equipped with two types of commercial membranes (Type I and Type II) supplied by Fujifilm Manufacturing Europe B.V: Type I Fuji membranes displayed higher Ohmic and non-Ohmic resistances than Type II membranes, which was mainly attributed to the difference in fixed charge density. The output power of the stack was observed to decrease with the increasing number of cell pairs mainly due to the increase in ionic shortcut currents. With the reduction in spacer thickness from 750 to 200 μm, the permselectivity of membranes in the stack decreased from 0.86 to 0.79 whereas the energy efficiency losses increased from 31% to 49%. Overall, the output of the present study provides a basis for understanding the impact of stack design on internal losses during the scaling-up of RED.

1 Introduction

Global energy consumption has increased dramatically in recent decades, with an expected increase of approximately 48% from 2012 to 2040 (Tufa et al., 2018b; Xue et al.,

✉ Corresponding authors
E-mail: wenjuanvivian@126.com (W. Zhang); changjinghit@163.com (J. Chang)

2020). Alternative clean and renewable energy resources are urgently required to alleviate the rising energy demand and associated environmental issues. Salinity gradient power (SGP) is a clean power resource generated by mixing water solutions. With the global potential being approximately 2.6 TW considering all the rivers worldwide flowing into the sea (Długołęcki et al., 2008), SGP presents one of the most promising, alternative renewable energy sources. Reverse electrodialysis (RED) allows for one-step conversion of salinity gradients into electrical current. In RED, a series of alternative cation exchange membranes (CEMs) and anion exchange membranes (AEMs) are configured between two electrodes, forming high concentration compartments (HCCs) and low concentration compartments (LCCs). By filling these compartments with the corresponding salt solutions, i.e, low concentration solution in the LCC and high concentration solution in the HCC, the salinity gradient induces the transport of anions and cations through AEMs and CEMs, respectively. This salinity gradient-driven ion transport is converted to electricity over electrodes by a redox reaction (Zhu et al., 2015).

In principle, the AEMs and CEMs could transport counterions with opposite charges while retaining co-ions with the same charge due to Donnan exclusion (Zhang et al., 2016a; Wang et al., 2019). The concentration polarization phenomenon results from the presence of a net charge on the membrane surface which influences the distribution of ions at the interface of the membrane and solution (Zhang et al., 2018). This leads to an increase in the counterion concentrations resulting in a thin (nanometer order) electrical double layer (EDL) (Długołęcki et al., 2010b). The transport of ions through the membrane from HCC to LCC results in a difference in flux between the co-ion and the counterion at the interface of the membrane and solution phase which results in a diffusion boundary layer (DBL). The DBL has a thickness on the order of hundreds of micrometers (Zhang et al., 2016a). The output of RED power is highly influenced by the electromotive potential over the stack and the internal stack resistance including Ohmic and non-Ohmic resistance (Vermaas et al., 2011). The Ohmic resistance is mainly ascribed to membrane resistance and solution resistance in the stack. The non-Ohmic resistance is mainly ascribed to EDL resistance and DBL resistance (Zhang et al., 2017), which can be discriminated by impedance spectroscopy (EIS), a powerful diagnostic electrochemical tool (Zhang et al., 2016b; Zhang et al., 2017).

The concept of RED was first proposed by Pattle in 1954 using a simple RED stack to generate electricity obtaining an output power of 25 mV/m (Pattle, 1954). The development then expanded to a broad range of topics including process analysis and testing (Post et al., 2009; Długołęcki et al., 2010a; Mehdizadeh et al., 2019), membrane and stack design (Guler et al., 2014; Gao et al., 2018), fouling(Rijnaarts et al., 2019), modeling and simulations (Gurreri et al., 2013), and integrated systems (Kim et al., 2013; Jande and Kim, 2014). Recently, advances toward large-scale RED developments have also been demonstrated. For instance, a pilot-scale RED with 125 cell pairs (44 cm × 44 cm) has been tested under an EU-FP7 REAPower project using brackish water and brine from saltworks (Tedesco et al., 2016).

Despite all the developments thus far, little effort has been made on the experimental (in situ) characterization of RED stack to quantify the Ohmic and non-Ohmic losses for different stack designs. Długołęcki et al. evaluated the impact of spacer shadow effects and concentration polarization on RED performance (Długołęcki et al., 2009). It was shown that the concentration polarization which can be influenced by optimal stack hydrodynamics significantly reduced the practical power output in RED. However, one strategy to reduce the spacer shadow effect is improving hydrodynamics, which implies the possible requirement of other strategies, such as new spacer designs. To better understand this phenomenon, more thorough investigations of RED stacks with different designs using different types of membrane materials and spacer properties remain crucial.

EIS measurements are typically carried out by applying alternating currents to the system and obtaining the response signals in the form of voltage or current. The ratio of the input and response variable forms the impedance spectra or admittance spectra, which can be interpreted by fitting to an equivalent circuit (Zhang et al., 2016a; Zhang et al., 2016b). The properties and contributions of each part in the system can be acquired using the EIS technique. EIS has been widely applied to investigate electrochemical processes, such as the dielectric and transport properties of membranes (Bason et al., 2007; Cen et al., 2015), membrane fouling processes (Ho et al., 2016; Jing and Chaplin, 2016), and electrochemical reaction rates. However, there have been no systematic investigations regarding the internal resistance and non-Ohmic resistance of RED stacks with different configurations using different types of membrane materials and spacer properties by in situ EIS measurements.

In the present work, the effect of stack configurations on the performance of RED was extensively studied by in situ EIS measurements. Special emphasis was given to Ohmic and non-Ohmic internal losses evaluated for stack design using two different types of membranes and three different types of spacer materials along with variations in the number of membrane cell pairs. Moreover, the trend in variations of permselectivity of membranes in RED stack and the energy efficiency losses were used to assess the impact of concentration polarization phenomenon and ‘spacer shadow effect’ on RED performance. The outputs of this work are expected to significantly contribute to (in situ) electrochemical characterization of RED stacks and quantification of internal losses, as well as identification of optimal stack designs for large scale implementation.

2 Theoretical basis

2.1 RED stack resistance

The internal resistance of the RED stack (R_S, Ω) is the sum of the Ohmic resistance (R_{Ohmic}, Ω) and non-Ohmic resistance ($R_{non\text{-}Ohmic}$, Ω):

$$R_S = R_{Ohmic} + R_{non\text{-}Ohmic}, \quad (1)$$

where R_{Ohmic} consists of the resistance of feed solutions (HCC and LCC), membranes (AEM and CEM) and electrode compartments.

$$R_{Ohmic} = \frac{N}{A}\left(R_{CEM} + R_{AEM} + \frac{d_{HC}}{\kappa_{HC}} + \frac{d_{LC}}{\kappa_{LC}}\right) + R_{el}, \quad (2)$$

where N is the number of cell pairs, A is the effective membrane area (cm^2); R_{CEM} and R_{AEM} are the area resistances of a single CEM and a single AEM ($\Omega \cdot m^2$), respectively; d_{HC} and d_{LC} are the thicknesses of HCC and LCC (m), respectively; κ_{HC} and κ_{LC} are the conductivities of HCC and LCC solutions (S/m), respectively, and R_{el} is the electrode resistance (Ω). $R_{non\text{-}Ohmic}$, which is ascribed to a stagnant DBL (R_{dbl}) and EDL (R_{edl}) on the electrodes, membrane interfaces and spacer interfaces, can be expressed as:

$$R_{non-Ohmic} = R_{edl} + R_{dbl}. \quad (3)$$

2.2 Open circuit voltage

The open circuit voltage (OCV) represents the maximum voltage obtained by the stack under zero current flow. The theoretical OCV for the RED stack can be calculated by the Nernst equation (Eq. (4)) (Długołęcki et al., 2008; Daniilidis et al., 2014; Tufa et al., 2014).

$$OCV_{theo} = N\frac{\alpha RT}{zF}\ln\left(\frac{a_{HC}}{a_{LC}}\right), \quad (4)$$

where OCV_{theo} is the theoretical OCV for the RED stack (V), N is the number of membrane cell pairs, R is the universal gas constant (8.314 J/(mol·K)), T is the absolute temperature (K), z is the electrochemical valence, F is the Faraday constant (96485 C/mol), a_{HC} and a_{LC} are the activities of the highly concentrated solution and dilute solution (M), respectively, and α is the average membrane permselectivity of an AEM and a CEM.

2.3 Stack power density

Power density (P_d, W/m^2) is an important parameter to characterize the RED stack. It can be expressed as below:

$$P_d = \left(\frac{E}{R_S + R_L}\right)^2 \frac{R_L}{A}, \quad (5)$$

where E is the electromotive force of the RED stack (V), and R_L is the external load resistance (Ω). The maximum power density ($P_{d,max}$) could be obtained when R_L equals to the internal resistance of the RED stack (R_S):

$$P_{d,max} = \frac{OCV^2}{4AR_S}. \quad (6)$$

2.4 Permselectivity and energy efficiency loss (EEL)

Permselectivity represents the ability of ion exchange membranes to selectively transport counterions through the membrane matrix (Długołęcki et al., 2008). The average apparent permselectivity of the ion exchange membranes in the RED stack (P_m) can be estimated by the ratio of the measured OCV and the theoretical OCV (OCV_{theo}) as follows:

$$P_m = \frac{OCV}{OCV_{theo}}. \quad (7)$$

To estimate the influence of the concentration polarization phenomenon and the spacer shadow effect, the parameter energy efficiency loss (EEL) is defined as:

$$EEL = \left(1 - \frac{P_{d,max}}{P_{d,theo}}\right) \times 100\%, \quad (8)$$

where $P_{d,theo}$ can be determined from the OCV_{theo} and the theoretical resistance of the RED stack. As mentioned by Dlugolecki et al.(2010), the theoretical resistance of the RED stack represented the lowest possible resistance for the stack with a specific configuration by excluding the spacer shadow effect and the concentration polarization phenomena. Essentially, this theoretical resistance is the Ohmic resistance obtained by EIS measurements.

3 Materials and methods

3.1 Membranes

Two commercial CEMs (CEM-Type I, CEM-Type II) and two AEMs (AEM-Type I and AEM-Type II) from Fujifilm manufacturing Europe B.V. (The Netherlands) were used in this study. Membrane samples were washed with deionized water three times followed by immersion in deionized water for at least 24 h before the test. The properties of the four ion exchange membranes are shown in Supporting Information (SI, Table S1).

3.2 Spacers

Three types of woven spacers (Sefar, Switzerland) with similar open areas and porosities were applied to investigate the effects of intermembrane distance on

RED performance. The properties of the spacers are shown in SI (Table S2). The morphology of spacers was observed by an optical microscope (Olympus BX-51, Japan).

3.3 Feed and electrolyte solutions

Feed solutions were prepared by dissolving reagent grade NaCl (Kermel, Tianjin) in deionized water. The concentration of the HCC solution was 0.5 mol/L and the concentration of the LCC solution was 0.05 mol/L. Feed solutions were pumped to the RED stack by gear pumps at a flow rate of 0.66 cm/s in the RED performance test and EIS measurements. Analytical grade $K_3Fe(CN)_6$ and $K_4Fe(CN)_6$ (Kermel, Tianjin) were used to prepare the electrode rinse solution composed of 0.1 mol/L $K_4Fe(CN)_6$, 0.1 mol/L $K_3Fe(CN)_6$ and 0.25 mol/L NaCl (the purpose of NaCl addition was to increase the solution conductivity in electrode compartments) dissolved in deionized water. The electrolyte solution was pumped through the cathode and anode compartments at a flow rate of 630 mL/min by a peristaltic pump through a continuous stirring.

3.4 RED setup

A schematic view of the RED stack is shown in SI (Fig. S1). Experiments on RED were carried out for different stack configurations presented in Table 1. All experiments were performed at 25°C and repeated three times.

3.5 Electrochemical measurements

3.5.1 LSV measurements

The current-voltage curves for the RED stack were recorded by using linear sweep voltammetry (LSV) performed at a scan rate of 5 mV/s, by applying a current in the range of 0−0.29 A to the stack using a potentiostat/galvanostat (Metrohm Autolab PARSTAT302N). The potentiostat/galvanostat was connected to the two electrodes of the RED stack with the anode and cathode serving as the working electrode and counter electrode, respectively.

3.5.2 EIS measurements

EIS experiments were carried out using a potentiostat/galvanostat combined with a frequency response analyzer (Metrohm Autolab PARSTAT302N) in the frequency range of 100000−0.01 Hz and an alternating voltage amplitude of 0.01 V at a rate of 50 frequencies/decade. The potentiostat/galvanostat was connected to the anode and cathode of the RED stack.

The equivalent circuit (Zhang et al., 2016a; Zhang et al., 2016b; Fontananova et al., 2017) used for the fitting of EIS measurements is shown in SI (Fig. S2). The EIS data as well as the fitting data of the RED stack with some different configurations (Table S4) can be found in SI (Fig. S2). The EIS fitting data are well-matched with the equivalent circuit model, because the Chi-square values (χ^2) for the RED stack are in the magnitude of 10^{-5}.

4 Results and discussion

4.1 Influence of membrane types

4.1.1 Influence of membrane types on RED performance

The average membrane permselectivity for AEM-Type I and CEM-Type I was 0.85 and the average membrane permselectivity for AEM-Type II and CEM-Type II was 0.96. These values were obtained from chronopotentiometric measurements using a six-compartment setup. The

Table 1 Configurations of the RED stack with a different type of membranes and spacers, and a varying of cell pairs

Configuration No.	Controlled parameter	Membrane	Spacer	Number of cell pairs	Flow velocity in HCC and LCC (cm/s)	Flow rate of electrolyte (mL/min)
1	Membrane type	Type I	PET-07-465/49	10	0.66	630
2		Type II				
3	Number of cell pairs	Type II	PET-07-465/49	5	0.66	630
4				8		
5				10		
6				12		
7				15		
8				18		
9	Spacer type	Type II	PET-07-1160/56	5	0.66	630
10			PET-07-465/49			
11			PET-07-265/53			

experimental data for the real transport number and permselectivity of ion exchange membranes as well as a schematic view of the chronopotentiometry test setup are shown in the SI (Figs. S3−S5).

The OCV values (Fig. 1(b)) and the $P_{d,\ max}$ (Fig. 1(d)) of Type I membranes were both lower than those of Type II membranes because Type I membranes exhibit lower transport numbers (t) and average permselectivity (P_m) (AEM-Type I: $t = 0.950$ and $P_m = 0.900$, CEM-Type I: $t = 0.900$ and $P_m = 0.800$) than Type II membranes (AEM-Type II: $t = 0.996$ and $P_m = 0.992$, CEM-Type II: $t = 0.960$ and $P_m = 0.920$). Type I membranes exhibited lower fixed charge density than Type II membranes (see Table S1), which was also responsible for the differences in OCV.

The current-voltage curves and power density of the two RED stacks as determined by LSV are displayed in Fig. 1. From the current-voltage curves (Fig. 1(a)), we can obtain the OCV values and the total resistance of the stack ($R_{S\text{-}LSV}$). In Figs. 1(c) and 1(d), the $P_{d,\ max}$ for Type II membranes were higher than those for Type I membranes. This is mainly related to two factors: i) higher transport properties and hence OCV of Type II membranes compared to Type I as discussed above, and ii) different membrane and interface resistance values of Type II membranes which will be discussed later.

4.1.2 Influence of membrane types on interface resistance

The resistance for the RED stack obtained from EIS ($R_{S\text{-}EIS}$) and LSV measurements is presented in Fig. 2. The $R_{S\text{-}LSV}$ and/or $R_{S\text{-}EIS}$ (Fig. 2(a)) was higher than the R_{Ohmic}, indicating that the internal stack resistance of RED includes not only the resistance of membranes and solutions but also the interface resistance (R_{edl} and R_{dbl}). This is consistent with the values of $R_{S\text{-}LSV}$ and $R_{S\text{-}EIS}$ which are approximately equal to the sum of R_{Ohmic}, R_{edl} and R_{dbl}. As observed in Fig. 2(b), R_{edl} in the stack with Type I membranes was lower than that with Type II membranes, which was consistent with the zeta potential results shown in Table 1. As the zeta potential relates to the charge distribution on the membrane surface (Xie et al., 2011), higher charge density on membrane surface could result in stronger interactions of the fixed ions with the mobile ions. This was in agreement with the results of our previous study (Zhang et al., 2016a). Regarding the interfacial resistances, R_{dbl} was significantly higher than R_{edl} due to the difference in the thickness of the DBL (micrometer scale) and EDL (nanometer scale). The contribution of the non-Ohmic resistance of the RED stack in the present study reaches up to 12% of the internal stack resistance. However, the R_{Ohmic} and the $R_{S\text{-}LSV}$

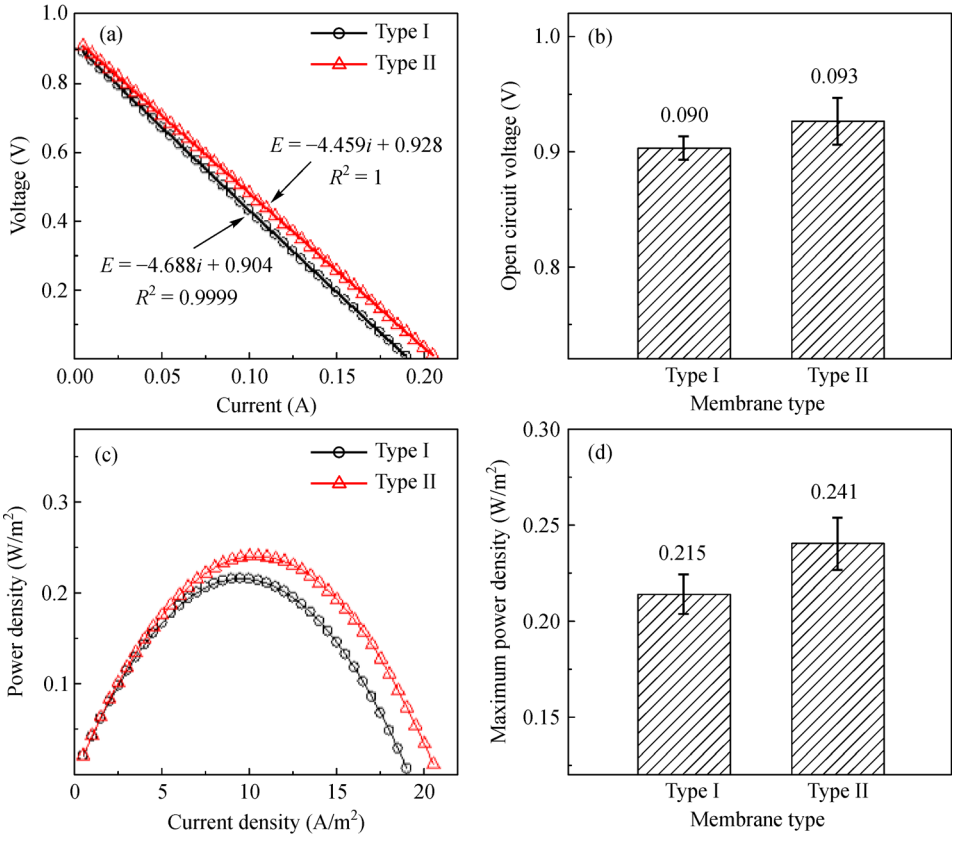

Fig. 1 (a) Voltage-current, (b) open circuit voltage, (c) power density curves and (d) maximum power density for the RED stack equipped with Type I and Type II ion exchange membranes; operating conditions: 10 cell pairs, flow velocity of 0.66 cm/s, spacer type of 07-465/49.

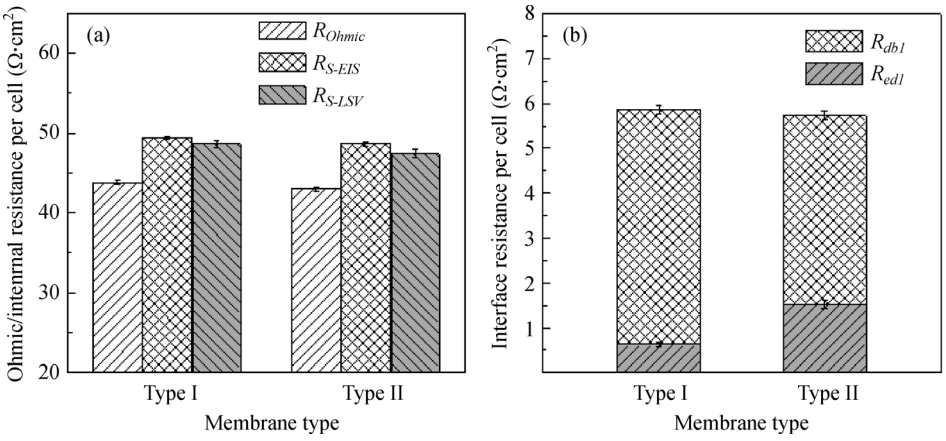

Fig. 2 The area resistance per cell of (a) Ohmic resistance (R_{Ohmic}) and stack resistance obtained from EIS measurements ($R_{S\text{-}EIS}$) as well as the stack resistance from LSV ($R_{S\text{-}LSV}$), and (b) the electrical double layer resistance (R_{edl}) and diffusion boundary layer resistance (R_{dbl}) of the RED stack with two types of ion exchange membranes. Operating conditions: 10 membrane cell pairs, flow velocity of 0.66 cm/s, 07-465/49 spacers.

(Fig. 2(a)) with Type I membranes were higher than those with Type II membranes, which was attributed to the higher thickness and lower fixed charge density (Table S1) in Type I membranes than that in Type II membranes.

4.2 Influence of the number of cell pairs

4.2.1 Influence of the number of cell pairs on RED performance

Figure 3 displays the variation in voltage and power density with current or current density and the number of cell pairs. The OCV increases linearly with the increase in the number of cell pairs (Fig. 3a and b). The equation from the linear regression of OCV ($OCV = 0.0919N$) shows that each "unit cell" (one pair of AEM-Type II and CEM-Type II together with one spacer) generates an OCV of 0.0919 V. This OCV value was lower than the OCV_{theo} (1.291 V) obtained by Eq. (4), which is ascribed to the effects of the concentration polarization phenomena and the spacer shadow effect in the stack.

As shown in Fig. 3(d), $P_{d,\ max}$ decreased with increasing number of cell pairs. The power density initially decreases when changing the number of cell-pairs from 5 to 7. Afterwards, the $P_{d,\ max}$ remains almost invariable. The initial decrease in $P_{d,\ max}$ can be related to the imminent impact of ionic shortcut currents with an increase in the number of cell pairs. Tufa *et al*. operated a pilot-scale RED unit (200 cell pairs) with feed solutions simulating SO_4^{2-}-rich industrial wastewater: the reported OCV and power density were generally low, which was claimed to be due to the manifestation of ionic shortcuts for a higher number of cell pairs (Tufa et al., 2018a), among other reasons. Moreover, Veerman et al.(2008)pointed out that the ionic shortcut currents formed by the ions migrating through inlet and outlet channels of the RED stack increase with an increasing number of cell pairs, which could cause a considerable loss of power efficiency.

4.2.2 Influence of the number of cell pairs on the stack and interface resistance

As shown in Fig. 4(a), the stack resistances ($R_{S\text{-}LSV}$ and/or $R_{S\text{-}EIS}$) and the R_{Ohmic} increased with increasing membrane cell pairs. The amounts of feed solutions and number of membranes increased with the number of cell pairs, thus leading to an increase in internal resistance in the RED stack (Eq. (2)). The compositions of the electrolytes in the electrode compartments did not change during the power generation process, so the internal resistance for the electrode compartment did not vary. The electrode resistance (blank resistance) can be obtained by linear regression of the R_{Ohmic} plot with the number of cell pairs (details are given in the Supporting Information). The obtained linear regression equation ($R = 0.436N + 0.259$), indicates that the blank resistance is approximately 0.259 Ω, and the resistance of the unit cell is 0.436 Ω. It is evident (Fig. 4(b)) that the resistances significantly increased with the increasing number of cell pairs, which resulted in an efficiency loss of RED stack. Nevertheless, the R_{edl} and R_{dbl} per cell decreased with increasing cell pairs (Fig. 4(d)). This may be related to the lower tightness and compression of the membranes in a single cell pair than numerous cell pairs which could influence the fluid turbulence and the thickness of the EDL and DBL.

Combining the fitting equations for OCV (Fig. 3(c)), stack resistance (Fig. S6 in Supporting Information) and Eq. (6), $P_{d,\ max}$ can be calculated as follows:

$$P_{d,max} = \frac{OCV^2}{4AR_S} = \frac{(0.0919N)^2}{0.04N \cdot (0.436N + 0.259)}. \quad (9)$$

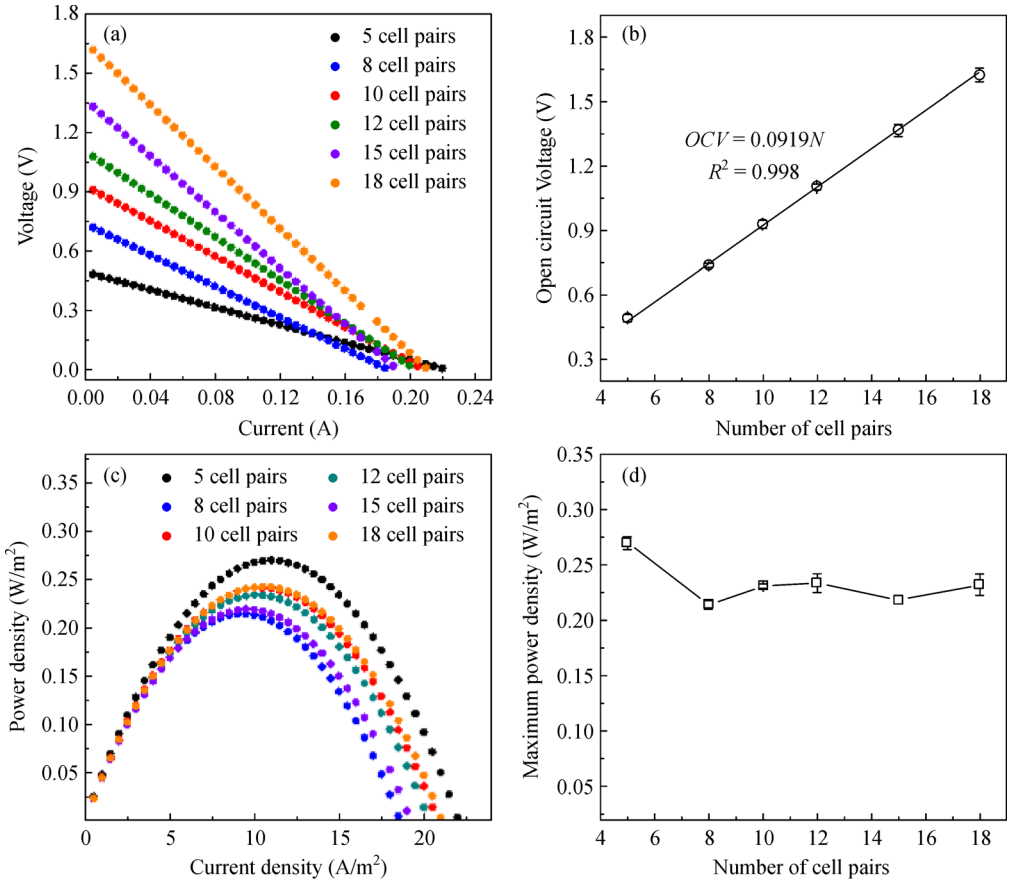

Fig. 3 (a) Voltage and (b) power density as a function of current, and (c) open circuit voltage and (d) maximum power density as a function of the number of cell pairs measured by LSV; operating conditions: flow velocity of 0.66 cm/s, 07-465/49 spacer, Type II membranes.

The fitting results can be applied to predict the electrochemical behaviors in large-scale RED systems. Equation (9), implies that the $P_{d,\ max}$ of the RED stack decreases gradually with the increase in number of cell pairs, which is consistent with our experimental data (Fig. 3(d)), and the decrease in $P_{d,\ max}$ is mainly attributed to the increasing number of cell pairs, as mentioned earlier. It has been concluded that the impact of ionic shortcut currents was less when the number of cell pairs was no more than 5 (Post et al., 2009; Veerman et al., 2009a; Veerman et al., 2011). However, in practical applications, RED stacks are assembled with large numbers of membranes to increase voltage and save space, so further study is required to clarify the scale on which ionic shortcut currents impact the efficiency loss.

4.3 Influence of intermembrane distance

4.3.1 Influence of intermembrane distance on RED performance

In the RED stack, spacers are used to separate membranes, construct respective channels for HCC solutions and LCC solutions, and promote mixing (Vermaas et al., 2014). The intermembrane distance which corresponds to spacer thickness is an important parameter for power efficiency in RED. A short intermembrane distance could result in a high pressure drop, whereas a long distance creates a high resistance over the compartments, leading to low net power output. In our study, three different types of spacers (Table S2) were selected to investigate the effects of intermembrane distance on RED equipped with AEM-Type II and CEM-Type II (5 cell pairs). Figure 5 shows the morphology of the three types of spacers.

The influences of spacer properties on *OCV* are shown in Figs. 6(a) and 6(b). The *OCV* in RED stacks increased from 0.474 to 0.513 V with increasing spacer thickness, which was in agreement with the report of Długołęcki et al. (2009). This was because the salt compartment with a thinner spacer had a relatively greater effect on the concentration polarization phemomena in the stack. In the current study, the ratios of interface to stack resistance ($R_{non\text{-}Ohmic}/R_{S\text{-}EIS}$) were 0.08, 0.13, and 0.22 for spacers 07-1160/56, 07-465/49, and 07-265/53 based on the fitting results of EIS measurements, revealing more severe concentration polarization in thinner spacers. Thus, the

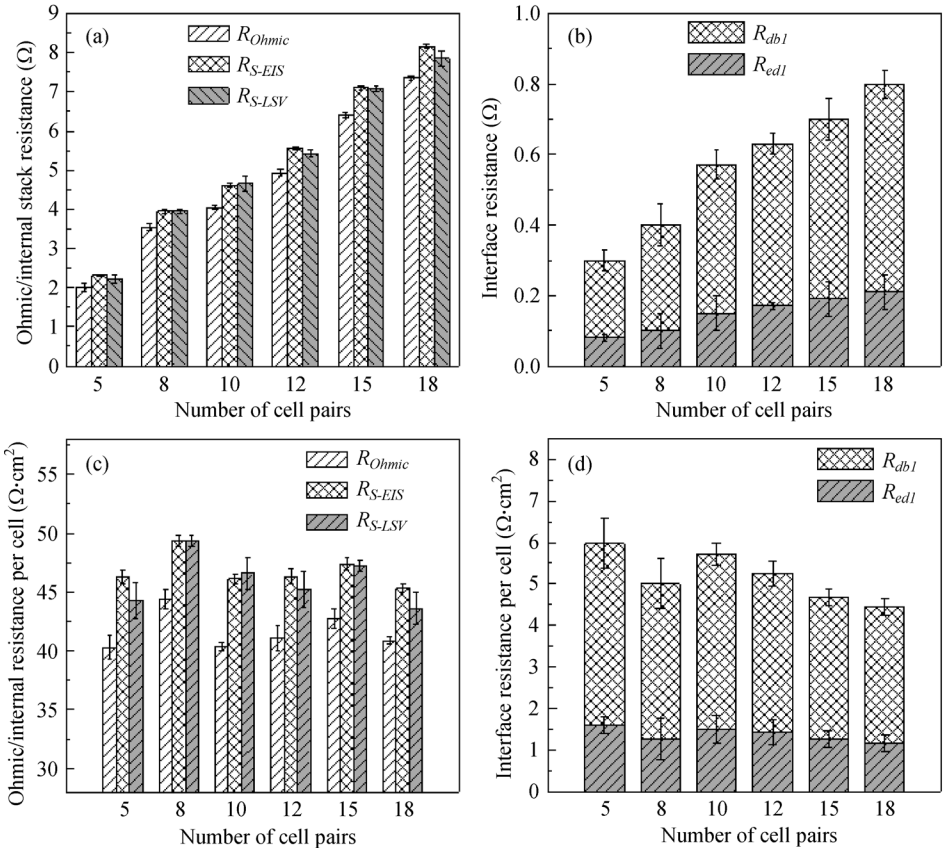

Fig. 4 The non-Ohmic resistance ($R_{non\text{-}Ohmic}$), electrical double layer resistance (R_{edl}) and diffusion boundary layer resistance (R_{dbl}) of the RED stack as a function of the number of cell pairs. Operating conditions: flow velocity of 0.66 cm/s, 07-465/49 spacer and Type II membranes.

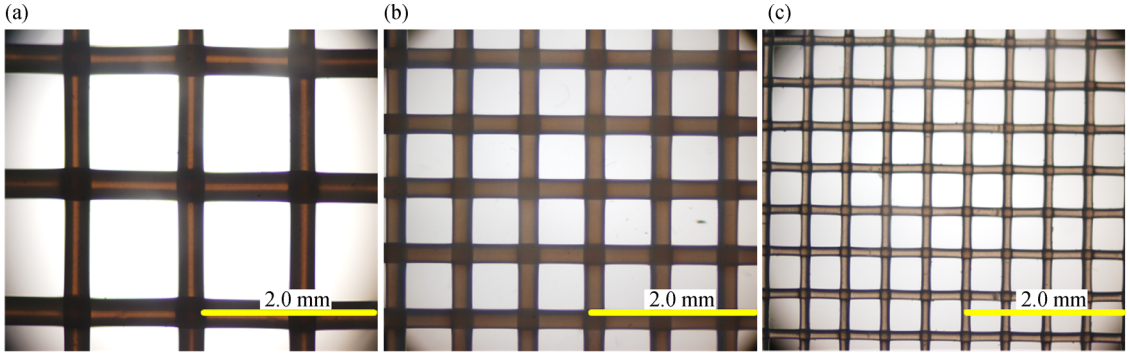

Fig. 5 The morphology of spacers. (a) 07-1160/56; (b) 07-465/49; (c) 07-265/53. Microscopic images taken at a magnification of 20. The largest opening size is for 07-1160/56 and the smallest for 07-265/53 with 07-465/49 in the middle.

improved *OCV* for greater spacer thickness can be explained by its ability to abate concentration polarization. Długołęcki et al. (2009) also found that the interface resistance caused by concentration polarization in the stack with a 0.2 mm spacer was higher than that with a 0.5 mm spacer, which can be minimized by increasing the linear solution flow rate. The maximum power density (Figs. 6(c) and 6(d)) increased by twofold (from 0.186 to 0.386 W/m^2) when reducing the intermembrane distance from 750 to 200 μm. Despite the more severe concentration polarization for thinner spacers, the smaller channel thickness would greatly reduce the Ohmic resistance (see Section 4.3.2) of the diluted compartment, thus increasing the maximum power density (Veerman et al., 2009a; Veerman et al., 2009b).

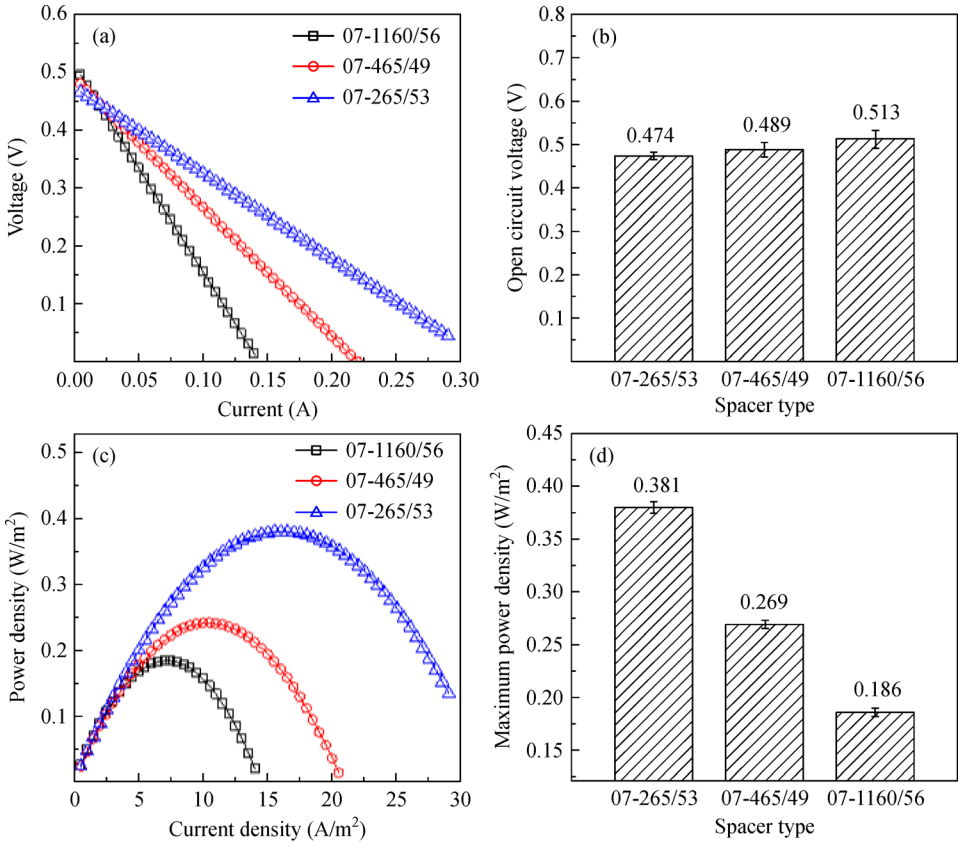

Fig. 6 Influences of spacer properties: (a) current-voltage curves, (b) OCV vs spacer type, (c) power curves, (d) maximum power density vs spacer type. Operating conditions: Type II membranes (5 cell pairs), flow velocity of 0.66 cm/s, HCC of 0.5 mol/L, and LCC of 0.05 mol/L.

4.3.2 Influence of intermembrane distance on the stack and interface resistance

Figure 7 shows the effect of spacer properties on stack resistance and interface resistance. The $R_{S\text{-}LSV}$ with thinner spacers numbered 07-465/49 and 07-265/53 was reduced by 38% and 59%, respectively, compared to that with spacers of 07-1160/56. Spacers with lower thickness resulted in shorter distances between membranes, especially for dilute compartments with low solution conductivity, indicating that spacer thickness had crucial effects on stack resistance. As shown in Fig. 5(b), the non-Ohmic resistances increased with decreasing intermembrane distance, which implied that thicker spacers could promote fluid turbulence in HCC and LCC, thus weakening the concentration polarization at the interface of the membrane and solution and reducing the mass transfer resistance at the interface of the membrane and solution in the stack.

4.4 Permselectivity study

The effects of membrane types, number of cell pairs and spacer properties on the average permselectivity of membranes in the stack and EEL are presented in Fig. 8. In general, the reported P_m values (as calculated by Eq. (7)) were low (Fig. 8(a)) which could be attributed to the pronounced 'spacer shadow effect' and the concentration polarization phenomenon in the stack. The P_m for the stack with Type I membranes was slightly lower than that of the Type II membranes, which is consistent with the lower P_m of Type I membranes (0.85) compared to Type II membranes (0.96). The spacer material used in our study was PET, a non-conductive material that could block ionic transport from the solution phase to the membrane. The efficiency loss due to the 'spacer shadow effect' and concentration polarization phenomenon for the two types of membranes was up to 40% (Fig. 8(b)).

In Fig. 8(c), the stack P_m and the *EEL* decreased with the increasing number of cell pairs. As was mentioned above the area resistance of the EDL and DBL (Fig. 4(d)) per cell pair decreased with increasing cell pair number, so the reduction in P_m and *EEL* was mainly attributed to the ionic shortcut currents.

In Fig. 8(d), the stack P_m decreased from 0.86 to 0.79 when the intermembrane distance was changed from 200 to 750 μm. As depicted in Section 4.3.1, the ratio of interface resistance and the stack resistance for the

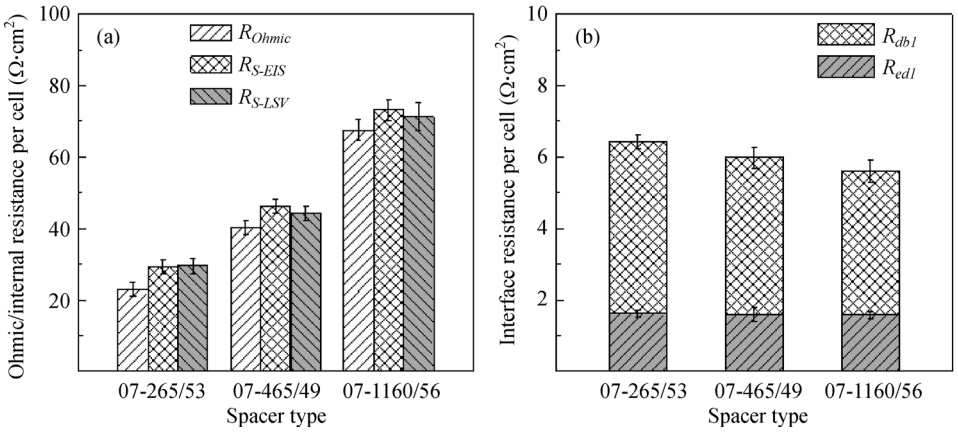

Fig. 7 Area resistance per cell for stack resistance obtained by EIS ($R_{S\text{-}EIS}$) and LSV ($R_{S\text{-}LSV}$), Ohmic resistance (R_{Ohmic}), electrical double layer resistance (R_{edl}) and diffusion boundary layer resistance (R_{dbl}) with different spacers. Operating conditions: Type II membranes (5 cell pairs), flow velocity of 0.66 cm/s, HCC of 0.5 mol/L and LCC of 0.05 mol/L.

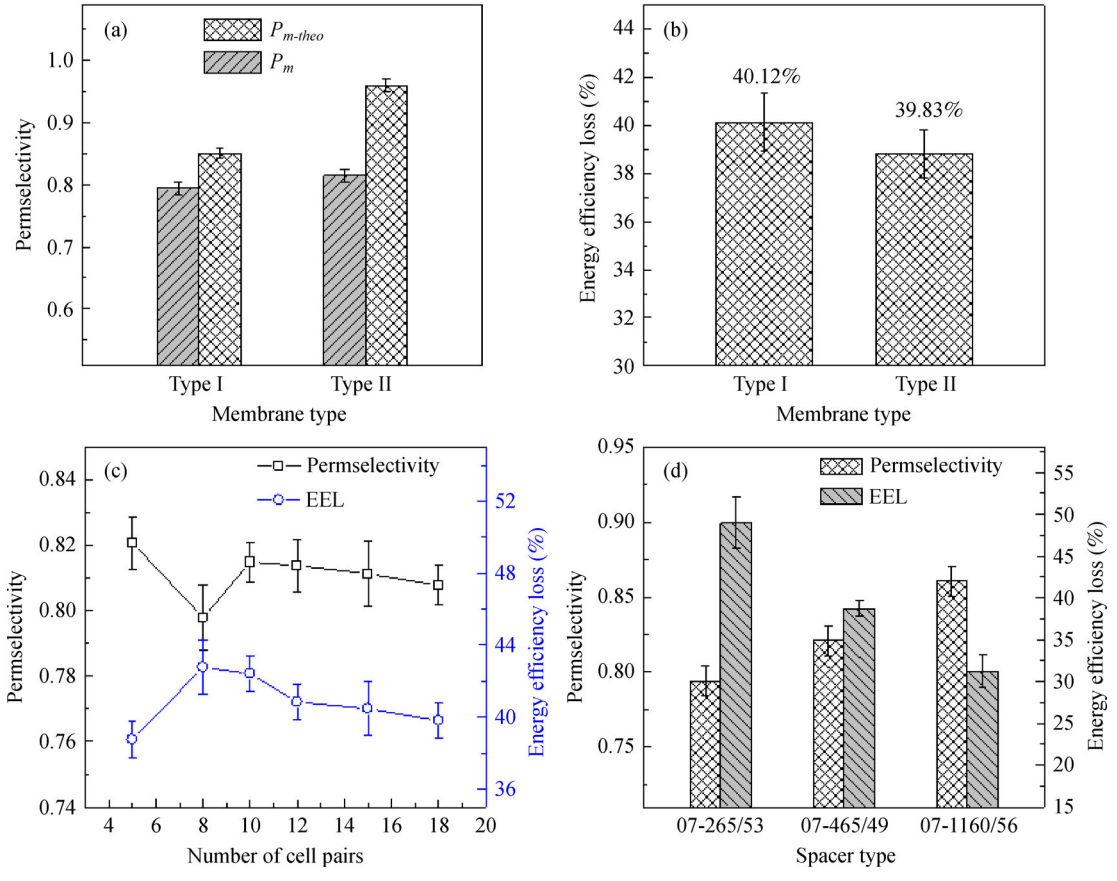

Fig. 8 (a) Average apparent permselectivity of membranes in the RED stack (P_m) and (b) the energy efficiency loss (*EEL*) as a function of membrane type; (c) P_m and *EEL* as a function of number of cell pairs; (d) P_m and *EEL* as a function of spacer type.

different spacer types increases from 0.10 to 0.19 with the decrease in spacer thickness from 750 to 200 μm, indicating the relatively greater effect of concentration polarization phenomena and the 'spacer shadow effect' in the stack with thinner spacers. A similar approach also explains the variations in *EEL*. Consequently, higher $P_{d,\ max}$ was obtained for the stacks with thinner spacers due to the dramatic reduction of the Ohmic resistance in

the stack, but higher *EEL* (49%) was attained as a result of the relatively greater effect of concentration polarization phenomena and the 'spacer shadow effect'.

5 Conclusions

In this study, extensive in situ EIS experimental characterization of RED was carried out for different stack configurations (2 types of membranes, 6 different variations in a number of cell pairs, 3 types of spacers). EIS, as a powerful technology, could distinguish between the interface resistances and the Ohmic resistance of the stack. Moreover, the effects of the concentration polarization phenomenon and 'spacer shadow effects' on the interface resistance as well as on the performance of the RED power output can be quantitatively analyzed. It was observed that higher OCV and higher maximum power density were obtained in the RED stack with Type II Fuji ion exchange membranes which had comparatively lower interface resistances and higher permselectivity than Type I Fuji ion-exchange membranes. The ionic shortcut current played an important role in the reduction of the maximum power density for a high number of cell pairs, which also concurrently resulted in lower stack permselectivity. The maximum power density increased twofold from 0.186 to 0.386 W/m^2 when reducing the intermembrane distance from 750 to 200 μm. However, the reduction in intermembrane distance with the decrease in spacer thickness from 750 to 200 μm results in the manifestation of the 'spacer shadow effect'. This leads to a reduction in the average apparent permselectivity of membranes in the stack from 0.86 to 0.79 and an increase in the energy efficiency loss from 31% to 49%. However, further investigation is required to clarify the ionic shortcut current effects and the trade-off between intermembrane distance or spacer geometry with concentration polarization and intermembrane distance on a much larger scale. This will be advantageous for the optimal design of large-scale RED systems and commercial implementations with Type II Fuji ion exchange membranes and with 07-265/53 spacers.

Acknowledgements The authors gratefully acknowledge the financial support from Tianjin Enterprise Science and Technology Commissioner Project (No. 19JCTPJC46900), Tianjin Municipal Education Commission Research Plan Projects (Nos.2018KJ161 and TJPU2k20170112), Tianjin Chengjian University research fund (No. 180501412), the National Key Research and Development Program of China (No. 2018YFC1903203), the Fundamental Research Funds for the Central Universities, China (2020CDJQY-A017), and Chongqing Technological Innovation and Application Development Project (No. cstc2019jscx-tjsbX0002). The work described in this paper was also partially supported by a grant from the Research Grants Council of the Hong Kong Special Administration Region, China (No. C7051-17G). Tao Lei from Metrohm China is also gratefully acknowledged for providing useful information about Metrohm Autolab potensiostat. The financial support of the European Union's Horizon 2020 research and innovation program under the Marie Skłodowska-Curie Actions IF Grant agreement (No. 748683) is gratefully acknowledged.

Electronic Supplementary Material Supplementary material is available in the online version of this article at https://doi.org/10.1007/s11783-021-1480-9 and is accessible for authorized users.

References

Bason S, Oren Y, Freger V (2007). Characterization of ion transport in thin films using electrochemical impedance spectroscopy: II: Examination of the polyamide layer of RO membranes. Journal of Membrane Science, 302(1–2): 10–19

Cen J, Vukas M, Barton G, Kavanagh J, Coster H G L (2015). Real time fouling monitoring with Electrical Impedance Spectroscopy. Journal of Membrane Science, 484: 133–139

Daniilidis A, Vermaas D A, Herber R, Nijmeijer K (2014). Experimentally obtainable energy from mixing river water, seawater or brines with reverse electrodialysis. Renewable Energy, 64: 123–131

Długołęcki P, Anet B, Metz S J, Nijmeijer K, Wessling M (2010a). Transport limitations in ion exchange membranes at low salt concentrations. Journal of Membrane Science, 346(1): 163–171

Dlugolecki P, Dabrowska J, Nijmeijer K, Wessling M (2010). Ion conductive spacers for increased power generation in reverse electrodialysis. Journal of Membrane Science, 347(1–2): 101–107

Długołęçki P, Gambier A, Nijmeijer K, Wessling M (2009). Practical potential of reverse electrodialysis as process for sustainable energy generation. Environmental Science & Technology, 43(17): 6888–6894

Długołęcki P, Nymeijer K, Metz S, Wessling M (2008). Current status of ion exchange membranes for power generation from salinity gradients. Journal of Membrane Science, 319(1–2): 214–222

Długołęcki P, Ogonowski P, Metz S J, Saakes M, Nijmeijer K, Wessling M (2010b). On the resistances of membrane, diffusion boundary layer and double layer in ion exchange membrane transport. Journal of Membrane Science, 349(1–2): 369–379

Fontananova E, Messana D, Tufa R A, Nicotera I, Kosma V, Curcio E, Van Baak W, Drioli E, Di Profio G (2017). Effect of solution concentration and composition on the electrochemical properties of ion exchange membranes for energy conversion. Journal of Power Sources, 340: 282–293

Gao H, Zhang B, Tong X, Chen Y (2018). Monovalent-anion selective and antifouling polyelectrolytes multilayer anion exchange membrane for reverse electrodialysis. Journal of Membrane Science, 567: 68–75

Güler E, Van Baak W, Saakes M, Nijmeijer K (2014). Monovalent-ion-selective membranes for reverse electrodialysis. Journal of Membrane Science, 455: 254–270

Gurreri L, Tamburini A, Cipollina A, Micale G, Ciofalo M (2013). CFD Simulation of Mass Transfer Phenomena in Spacer Filled Channels for Reverse Electrodialysis Applications. Icheap-11: 11th International Conference on Chemical and Process Engineering, Pts 1–4, 32: 1879–1884

Ho J S, Low J H, Sim L N, Webster R D, Rice S A, Fane A G, Coster H G L (2016). In-situ monitoring of biofouling on reverse osmosis membranes: Detection and mechanistic study using electrical

impedance spectroscopy. Journal of Membrane Science, 518: 229–242

Jande Y A C, Kim W S (2014). Integrating reverse electrodialysis with constant current operating capacitive deionization. Journal of Environmental Management, 146: 463–469

Jing Y, Chaplin B P (2016). Electrochemical impedance spectroscopy study of membrane fouling characterization at a conductive sub-stoichiometric TiO_2 reactive electrochemical membrane: Transmission line model development. Journal of Membrane Science, 511: 238–249

Kim J, Kim S J, Kim D K (2013). Energy harvesting from salinity gradient by reverse electrodialysis with anodic alumina nanopores. Energy, 51: 413–421

Mehdizadeh S, Yasukawa M, Abo T, Kakihana Y, Higa M (2019). Effect of spacer geometry on membrane and solution compartment resistances in reverse electrodialysis. Journal of Membrane Science, 572: 271–280

Pattle R E (1954). Production of electric power by mixing fresh and salt water in the hydroelectric pile. Nature, 174(4431): 660

Post J W, Hamelers H V M, Buisman C J N (2009). Influence of multivalent ions on power production from mixing salt and fresh water with a reverse electrodialysis system. Journal of Membrane Science, 330(1–2): 65–72

Rijnaarts T, Moreno J, Saakes M, De Vos W M, Nijmeijer K (2019). Role of anion exchange membrane fouling in reverse electrodialysis using natural feed waters. Colloids and Surfaces. A, Physicochemical and Engineering Aspects, 560: 198–204

Tedesco M, Scalici C, Vaccari D, Cipollina A, Tamburini A, Micale G (2016). Performance of the first reverse electrodialysis pilot plant for power production from saline waters and concentrated brines. Journal of Membrane Science, 500: 33–45

Tufa R A, Curcio E, Van Baak W, Veerman J, Grasman S, Fontananova E, Di Profio G (2014). Potential of brackish water and brine for energy generation by salinity gradient power-reverse electrodialysis (SGP-RE). RSC Advances, 4(80): 42617–42623

Tufa R A, Hnát J, Němeček M, Kodým R, Curcio E, Bouzek K (2018a). Hydrogen production from industrial wastewaters: An integrated reverse electrodialysis—Water electrolysis energy system. Journal of Cleaner Production, 203: 418–426

Tufa R A, Pawlowski S, Veerman J, Bouzek K, Fontananova E, Di Profio G, Velizarov S, Goulão Crespo J, Nijmeijer K, Curcio E (2018b). Progress and prospects in reverse electrodialysis for salinity gradient energy conversion and storage. Applied Energy, 225: 290–331

Veerman J, De Jong R M, Saakes M, Metz S J, Harmsen G J (2009a). Reverse electrodialysis: Comparison of six commercial membrane pairs on the thermodynamic efficiency and power density. Journal of Membrane Science, 343(1–2): 7–15

Veerman J, Post J W, Saakes M, Metz S J, Harmsen G J (2008). Reducing power losses caused by ionic shortcut currents in reverse electrodialysis stacks by a validated model. Journal of Membrane Science, 310(1–2): 418–430

Veerman J, Saakes M, Metz S J, Harmsen G J (2009b). Reverse electrodialysis: Performance of a stack with 50 cells on the mixing of sea and river water. Journal of Membrane Science, 327(1–2): 136–144

Veerman J, Saakes M, Metz S J, Harmsen G J (2011). Reverse electrodialysis: A validated process model for design and optimization. Chemical Engineering Journal, 166(1): 256–268

Vermaas D A, Saakes M, Nijmeijer K (2011). Power generation using profiled membranes in reverse electrodialysis. Journal of Membrane Science, 385–386: 234–242

Vermaas D A, Saakes M, Nijmeijer K (2014). Enhanced mixing in the diffusive boundary layer for energy generation in reverse electrodialysis. Journal of Membrane Science, 453: 312–319

Wang X, Li N, Li J, Feng J, Ma Z, Xu Y, Sun Y, Xu D, Wang J, Gao X, Gao J (2019). Fluoride removal from secondary effluent of the graphite industry using electrodialysis: Optimization with response surface methodology. Frontiers of Environmental Science & Engineering, 13(4): 51

Xie H, Saito T, Hickner M A (2011). Zeta potential of ion-conductive membranes by streaming current measurements. Langmuir, 27(8): 4721–4727

Xue W, Zaw M, An X, Hu Y, Tabucanon S (2020). Sea salt bittern-driven forward osmosis for nutrient recovery from black water: A dual waste-to-resource innovation via the osmotic membrane process. Frontiers of Environmental Science & Engineering, 2020, 14(2): 32

Zhang B, Hong J G, Xie S, Xia S, Chen Y (2017). An integrative modeling and experimental study on the ionic resistance of ion-exchange membranes. Journal of Membrane Science, 524: 362–369

Zhang W, Ma J, Wang P, Wang Z, Shi F, Liu H (2016a). Investigations on the interfacial capacitance and the diffusion boundary layer thickness of ion exchange membrane using electrochemical impedance spectroscopy. Journal of Membrane Science, 502: 37–47

Zhang W, Wang P, Ma J, Wang Z, Liu H (2016b). Investigations on electrochemical properties of membrane systems in ion-exchange membrane transport processes by electrochemical impedance spectroscopy and direct current measurements. Electrochimica Acta, 216: 110–119

Zhang Y, Liu R, Lang Q, Tan M, Zhang Y (2018). Composite anion exchange membrane made by layer-by-layer method for selective ion separation and water migration control. Separation and Purification Technology, 192: 278–286

Zhu X, He W, Logan B E (2015). Reducing pumping energy by using different flow rates of high and low concentration solutions in reverse electrodialysis cells. Journal of Membrane Science, 486: 215–221